Force and focal adhesion assembly: a close relationship studied using elastic micropatterned substrates

Nathalie Q. Balaban*, Ulrich S. Schwarz†, Daniel Riveline‡, Polina Goichberg*, Gila Tzur*, Ilana Sabanay*, Diana Mahalu§, Sam Safran†, Alexander Bershadsky*, Lia Addadi¶ and Benjamin Geiger*#

**Department of Molecular Cell Biology, The Weizmann Institute of Science, Rehovot, Israel*
†Department of Materials and Interfaces, The Weizmann Institute of Science, Rehovot, Israel
‡Laboratoire de Spectrometrie Physique, Universite Joseph Fourier, Grenoble, France
§Braun Center for Submicron Semiconductor Research, The Weizmann Institute of Science, Rehovot, Israel
¶Department of Structural Biology, The Weizmann Institute of Science, Rehovot, Israel
#e-mail: benny.geiger@weizmann.ac.il

Mechanical forces play a major role in the regulation of cell adhesion and cytoskeletal organization. In order to explore the molecular mechanism underlying this regulation, we have investigated the relationship between local force applied by the cell to the substrate and the assembly of focal adhesions. A novel approach was developed for real-time, high-resolution measurements of forces applied by cells at single adhesion sites. This method combines micropatterning of elastomer substrates and fluorescence imaging of focal adhesions in live cells expressing GFP-tagged vinculin. Local forces are correlated with the orientation, total fluorescence intensity and area of the focal adhesions, indicating a constant stress of 5.5 ± 2 nNμm-2. The dynamics of the force-dependent modulation of focal adhesions were characterized by blocking actomyosin contractility and were found to be on a time scale of seconds. The results put clear constraints on the possible molecular mechanisms for the mechanosensory response of focal adhesions to applied force.

Cell adhesion plays a critical role in many fundamental processes such as embryonic morphogenesis, angiogenesis, inflammation and wound healing[1–3]. One of the unique features of adhesion to a rigid surface, unlike binding to soluble ligands, is the ability of forces to develop at the contact site. Such forces can be external, such as shear flow in blood vessels, or can be generated by the cell's own contractile apparatus. There is a close relationship between the abilities of cells such as fibroblasts to generate force and to assemble matrix adhesions[4–7].

The primary sites of cell adhesion to the substrate are focal adhesions. These complex multimolecular assemblies link the extracellular matrix, via membrane-bound receptors, to the cell's cytoskeleton[8,9]. Focal adhesions are therefore also the sites at which forces are transmitted to the substrate. They can be detected as dark areas in interference reflection microscopy[10], by electron microscopy or with fluorescence labelling of specific adhesion molecules such as vinculin, paxillin and integrins. It has been recently shown that tension 'reinforces' focal adhesions[11], which are stimulated to grow after the application of a local external force[12]. Does the cell use its own contractility to reinforce its adhesion sites in a local targeted process? If so, the force applied at focal adhesions should determine their assembly. With this in mind, we explored the possibility that the mechanosensory response of focal adhesions is involved in autoregulation of their development. This was achieved by quantitatively mapping the relationships between the force applied at single focal adhesions and the assembly of the adhesion sites.

Several methods have been developed for measuring the forces that cells exert on their substrate, mainly involving the use of deformable substrates[13–17]. On the wrinklable substrates introduced by Harris[13], the tangential forces exerted by the cell are translated into out-of-plane wrinkles. More quantitative approaches to force measurements included the use of cantilevers[15], an improvement of the wrinklable substrate[17,18] and elastomer substrates of either prestressed thin polymer films[14] or thick polymer gels[16]. These methods provided quantitative evaluations of the forces, and some combined this with visualization of the adhesion sites[18]. Their capacity to compare the forces applied at the various focal adhesions of a cell is, however, limited.

To measure the forces exerted by single focal adhesions directly in real time and in live cells, we have developed a novel method based on the simultaneous visualization of the displacements (using a high-resolution micropatterned transparent elastomer) and the corresponding focal adhesions (using a green-fluorescent-protein (GFP) fusion protein of vinculin). The force applied by the cell to the substrate was calculated down to the level of a single adhesion site using elasticity theory, based on the measured displacements and the locations of the focal adhesions.

Mature focal adhesions are elongated structures, mostly oriented in the direction of the main stress fibres. We found that the direction of the force applied at each focal adhesion correlates with the main axis of this elongation. Furthermore, the measured local forces are linearly related to the total fluorescence intensity and area of GFP–vinculin at the respective focal adhesions. The linear dependence shows that a constant stress is applied by the cell at its various focal adhesions, despite large variations in their area and shape, as well as in the force applied to them. By interfering with the actomyosin-driven contractility of the cell, we monitored the force relaxation together with the dynamics of the focal adhesions. The disruption of the focal adhesions was found to follow closely the relaxation of force. The results suggest that the force the cell exerts, via actomyosin contraction, at its focal adhesion determines their assembly, on a time scale below seconds.

Results

The patterning method developed (see Methods) allowed the production of shallow patterns with a depth of 0.3 μm on the upper surface of the elastomer (Fig. 1a, d). The pattern could be visual-

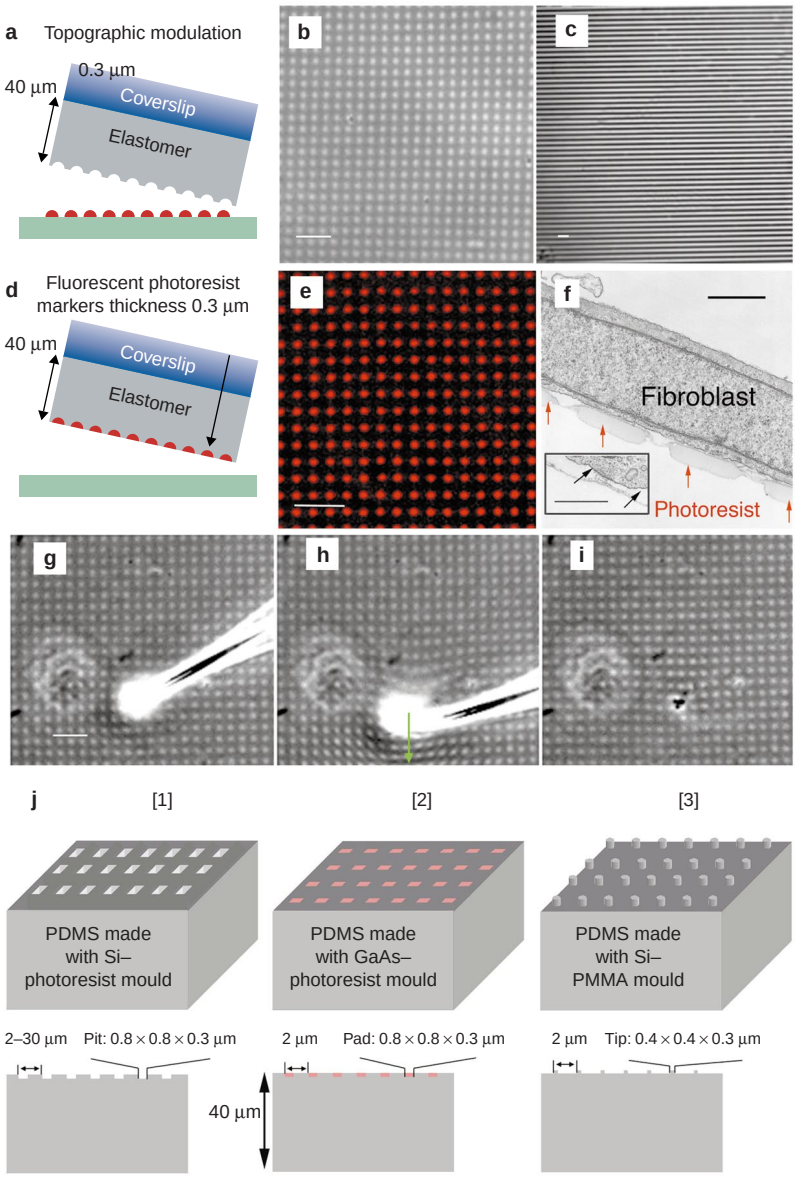

Figure 1 **Fabrication and calibration of the patterned elastomer. a**, Peeling off the elastomer from the Si mould results in a topographic modulation with a depth of 0.3 µm. **b**, Phase-contrast image of a pattern of dots obtained with Si moulds. **c**, Phase-contrast image of a pattern of lines obtained with Si moulds. **d**, Peeling off the elastomer from the GaAs mould results in the embedding of the photoresist pattern (seen as small dots) in the upper layer of the elastomer. **e**, Fluorescent image of the embedded photoresist dots. Bars **a–e** = 6 µm. **f**, Transmission electron microscopy image of a human foreskin fibroblast on top of the embedded fluorescent photoresist (red arrows). Bar = 1 µm. Inset: a focal adhesion (between black arrows) on the elastomer. Bar = 0.5 µm. **g**, Phase-contrast image of the calibration of the patterned elastomer (Young's modulus = 19 kPa) before pulling and (**h**) while pulling with a force of 450 nN. Notice the deformation of the regular pattern in the vicinity of the pipette. **i**, After relaxation. Bar = 6 µm. **j**, Different moulds result in different elastomer topography. 1, Small square pits of 0.8 µm width and 0.3 µm depth, with pattern size ranging from 2 µm to 30 µm. 2, Flat topography with embedded fluorescent photoresist markers (red boxes). 3, Small tips of 0.4 µm diameter and 0.3 µm height defined using electron-beam lithography. The bottom panels show the cross sections of the respective elastomers through the pattern. PDMS, polydimethylsiloxane; PMMA, polymethylmethacrylate.

ized by phase contrast (Fig. 1b, c) or fluorescence (Fig. 1e) microscopy. The Young's modulus of the elastomer was determined by monitoring the displacements in the pattern produced by micropipettes of known flexibility (Fig. 1g, h; see Methods). The pattern size (2–30 µm) and shape were chosen according to the spatial resolution of displacements needed. Large pitch patterns (Fig. 2a, b) were used to get a rapid semiquantitative evaluation of the generation of force in the culture, without need for a reference to the unstressed pattern. More precise measurements of the displacements were performed with the finer pattern (Fig. 1b, e), consisting in an array of small dots with diameter ~0.8 µm and pitch of 2 µm. Patterns of widely differing size and topography were tested (Fig. 1j). The forces and focal adhesions of the cells were, however, similar in the various patterns.

Human foreskin fibroblasts transiently expressing GFP–vinculin were plated on the patterned elastomer substrates, to determine the locations of the focal adhesions. The cells spread, develop focal adhesions (Fig. 1f) and proliferate on these substrates, similar to their behaviour on glass coverslips. The forces applied by the cells deform the initially regular pattern of the surface. The position

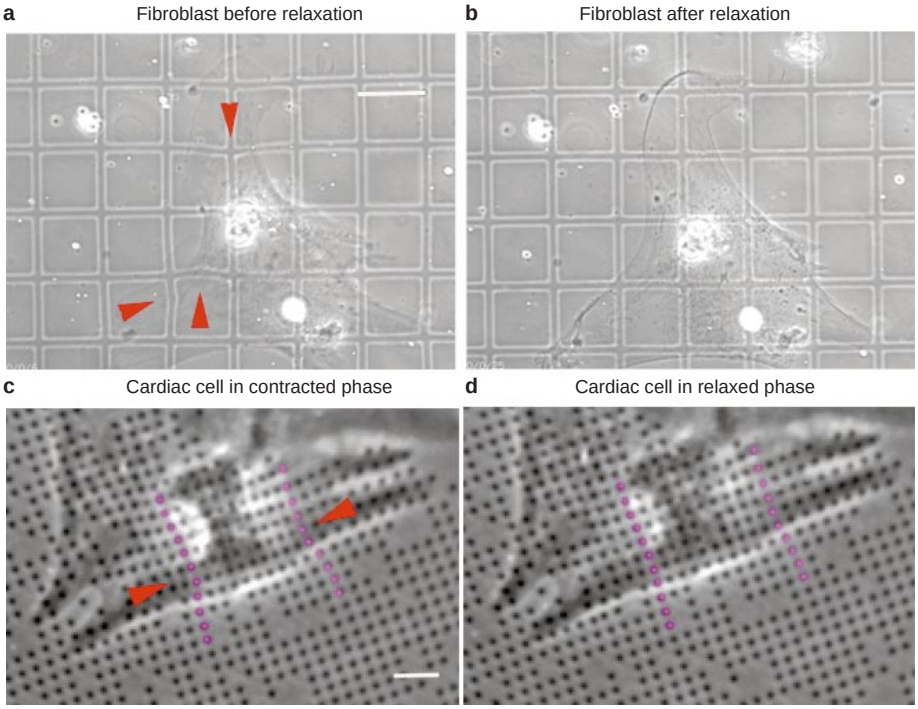

Figure 2 **Cells plated on the patterned elastomer create distortions.** **a**, Phase-contrast image of a rat cardiac fibroblast plated on a large grid pattern. The cell creates distortions (arrowheads) by applying force to the elastomer (Young's modulus = 18 kPa). **b**, The same cell as in a 10 min after BDM-induced relaxation. Notice the recovery of the regular grid pattern. Grid pitch = 30 μm. **c**, Phase-contrast image of a contracting cardiac myocyte plated on elastomer with embedded photoresist pattern of dots (Young's modulus = 19 kPa, bar = 6 μm). The dots can be clearly seen even under thick parts of the cell. The arrowheads and the magenta dots underline the pinching action of the contraction on the elastomer. Grid pitch = 2 μm. **d**, Relaxed phase.

of the centre of the dots is recorded together with the fluorescence picture of the focal adhesions, marked by GFP–vinculin, using a high-resolution fluorescence imaging system connected to a computer interface[19]. Using this system, it has previously been shown that the local intensity of the GFP-tagged proteins such as vinculin, paxillin and tensin is proportional to their levels in focal adhesions as revealed by immunofluorescence labelling[20]. The undistorted pattern is regular and so any deviation from regularity indicates an application of force. Full recovery of the regular pattern was confirmed by removing the cells from the substrate with trypsin. The displacements of the dots relative to their original position are determined using the 'water' algorithm[20] for automatic detection of the dot centre. Once the displacements are mapped (Fig. 3a, c), the forces generated at each focal adhesion are computed using elasticity theory for the semi-infinite space[21] (Fig. 3a, b). The only assumption included in the computation of the force pattern that fits the measured displacements is that the forces originate from the measured locations of the focal adhesions (see Methods). This assumption was supported by the fact that, on all the cells studied ($n = 40$), displacements were never observed in areas without well-developed focal adhesions.

To test possible cell-type-specific variability in focal-adhesion-mediated traction, we have examined elastomer deformation by highly contractile cardiac myocytes. The cells were isolated from neonatal rat hearts (see Methods) and directly plated on patterned elastomer substrates covered with fibronectin. Two days after plating, beating of many cells was observed at ~1 Hz frequency. Cells were recorded in the contracted (Fig. 2c) or relaxed (Fig. 2d) phase (see Supplementary Information). The red arrows and the magenta dots emphasize the pinching motion of the dots under the cell as it contracts. In many cells, contraction of the dorsal side was noted, without significant deformation of the substrate. Considerable deformation of the substrate occurred only in those cells whose contractile apparatus was anchored to the substrate by large focal adhesions, associated with the termini of contractile sarcomeric actin bundles. After observation of beating activity, the cardiac myocytes were fixed, permeabilized and stained for vinculin and actin, to visualize focal adhesions and the contractile apparatus. The analysis of the force applied to the substrate during beating was performed as described above for fibroblasts. The vinculin pattern of focal adhesions in cardiac myocytes was, however, often too dense to allow the resolution of distinct focal adhesions. Forces were therefore taken as applied by groups of vinculin-rich adhesions (Fig. 4).

In human foreskin and cardiac fibroblasts, the force applied at single focal adhesions varied from below the noise level to 30 nN. The area of vinculin or paxillin containing focal adhesions was variable too, ranging from small ($<1\ \mu m^2$) dots resembling focal complexes[22] to ~10 μm^2. Only focal adhesions with a centre-to-centre separation of at least 3 μm from other focal adhesions were measured. Comparison of the local traction force to the dimensions of individual focal adhesions shows a correlation between the force and the area or total intensity of the focal adhesions (Fig. 5a, b). The orientation of the force is also correlated with that of the focal adhesion (Fig. 5c), indicating that the increase in area owing to force is not isotropic but is mainly in the direction of force application.

In cardiac myocytes, the direction of the force is also parallel to the direction of the long axis of the focal adhesions, namely parallel to the sarcomeric apparatus (Fig. 4). We analysed the total force applied within a defined area, as well as the total area of the vinculin-rich patches. As expected for myocytes, the forces (~70 nN) in a given cell area were higher than the corresponding forces in fibroblasts (~20 nN). However, the total area of the vinculin-rich

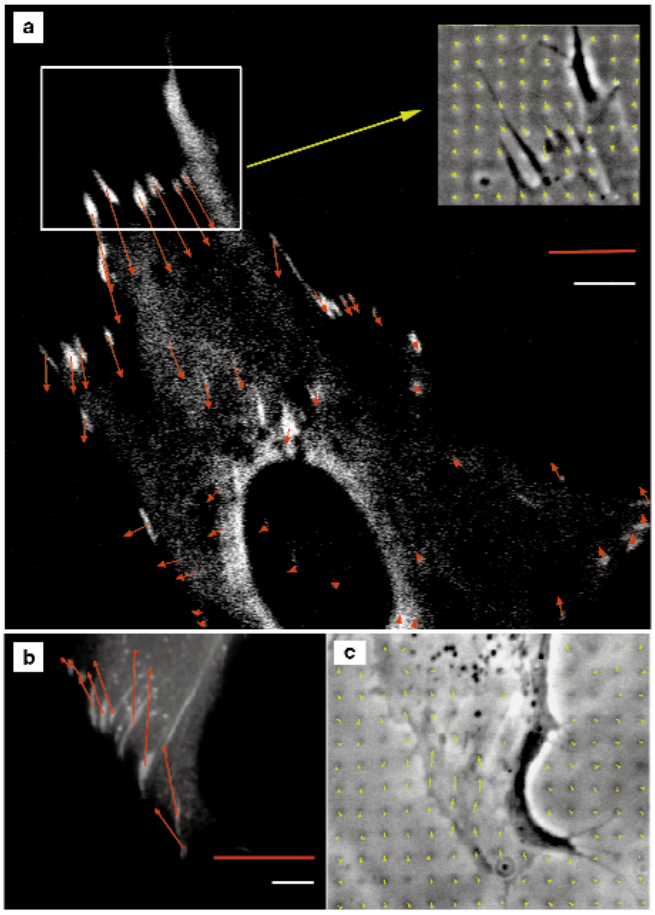

Figure 3 **Visualization of forces and focal adhesions. a**, Fluorescence image of a human foreskin fibroblast expressing GFP–vinculin, which localizes to focal adhesions. Red arrows correspond to forces extracted from the displacements of the patterned elastomer (Young's modulus = 18 kPa). Note the alignment of force with the direction of elongation of large focal adhesions. Inset, phase-contrast image of the upper part of the cell (white rectangle), showing displacements of the dots (green arrows); the pattern consists of small square pits (see Fig. 1j, 1). **b**, Fluorescence image of a human foreskin fibroblast stained with antibodies against paxillin, which also localizes at focal adhesions. Red arrows correspond to forces extracted from the displacements of the patterned elastomer (Young's modulus = 21 kPa); the pattern consists of small tips formed by electron-beam lithography (see Fig. 1j, 3). **c**, Phase-contrast image of the same cell immediately before fixation. White scale bars represent 4 μm; red scale bars represent 30 nN.

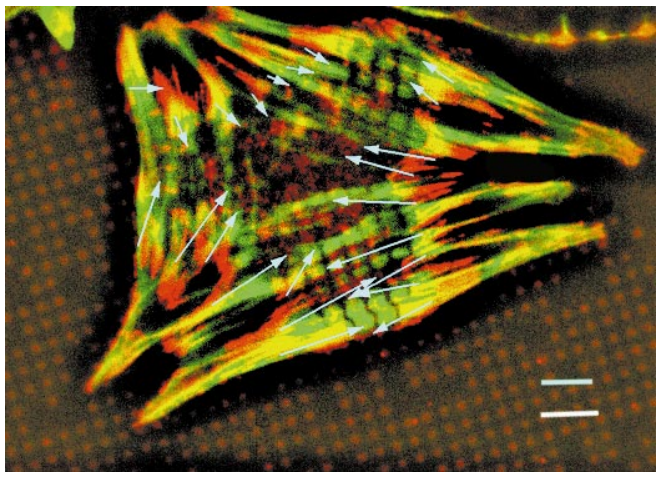

Figure 4 **Distribution of forces in a cardiac myocyte.** After recording the displacements of the pattern caused by beating (Fig. 2c, d), the cardiac myocytes are stained for vinculin (red) to visualize the sites of force transmission, and for actin (green). Yellow regions correspond to overlap of actin and vinculin. The light-blue arrows denote the forces applied to the substrate at the vinculin-rich areas. White bar = 6 μm; blue bar = 70 nN.

patches was also significantly higher. The ratio of these parameters (the stress) was found to vary between 2 nN μm^{-2} and 5 nN μm^{-2}. This value is similar to the one measured in focal adhesions of fibroblasts, as discussed below.

The simultaneous visualization, in live cells, of each focal adhesion and of the associated force (Fig. 5a–d) makes it possible to monitor the dynamics of the system. To establish the relationship between changes in the assembly of the structure and force over time, 2,3-butanedione monoxime (BDM, a known inhibitor of actomyosin contraction[23]) was added to fibroblasts. The time dependence of the relaxation of the forces was then recorded, together with the disruption of the focal adhesions (Fig. 5e–h). The illumination time was minimized in order to avoid bleaching. The relaxation of the matrix is apparent within seconds after the application of BDM. The relationship between force and area in all focal adhesions at all time points is plotted in Fig. 5e (each symbol represents a different focal adhesion). The correlation seen at $t = 0$ (Fig. 5a) is now more apparent and the determined linear dependence defines a constant stress, $P_f = 5.5 \pm 2$ nN μm^{-2}, applied at the focal adhesions. Extrapolation of this linear dependence to zero force shows that the tension-independent area of focal adhesions is ~1 μm^2. This residual area is similar to the typical size of focal complexes, which are the precursors of the larger adhesions formed once force is applied[12].

The time dependence of the force (red squares) and the total GFP–vinculin intensity (black circles) of a single focal adhesion after BDM treatment are plotted in Fig. 5f. The correlation between the two parameters is evident. The dynamic behaviour of single focal adhesions is consistent with the dependence found when plotting different adhesions at $t = 0$. Applying BDM is thus equivalent to moving the force axis at $t = 0$. A close correlation between force and total intensity is found for the various focal adhesions, as shown in Fig. 5g, which plots the average values obtained for all the single, spatially separated adhesions ($n = 10$) from Fig. 5d, h. The time dependence of the disassembly of focal adhesions after BDM is very similar to the force relaxation (Fig. 5f, g). Thus, the relaxation of actomyosin contraction is rapidly followed by the disruption of focal adhesions, while maintaining the linear dependence of focal adhesion assembly on force.

Discussion

A novel approach was developed, allowing a real-time and direct measurement of forces applied by stationary cells to the underlying matrix at individual focal adhesions. This approach was used to investigate the relationship between local forces at focal adhesions and their assembly. The area and total intensity of the focal adhesions are found to be linearly dependent on the local force applied by the cell. Furthermore, the time dependence of this relation is found to be below a few seconds. The linear dependence between force and area of the focal adhesion shows that a constant stress is applied to the various focal adhesions of the cell. Thus, the force applied by the cell on its substrate is closely linked to the assembly of the adhesion sites.

The measurements were performed on cells expressing GFP derivatives of specific focal adhesion molecules, cultured on micropatterned elastic substrates. The displacements of the pattern

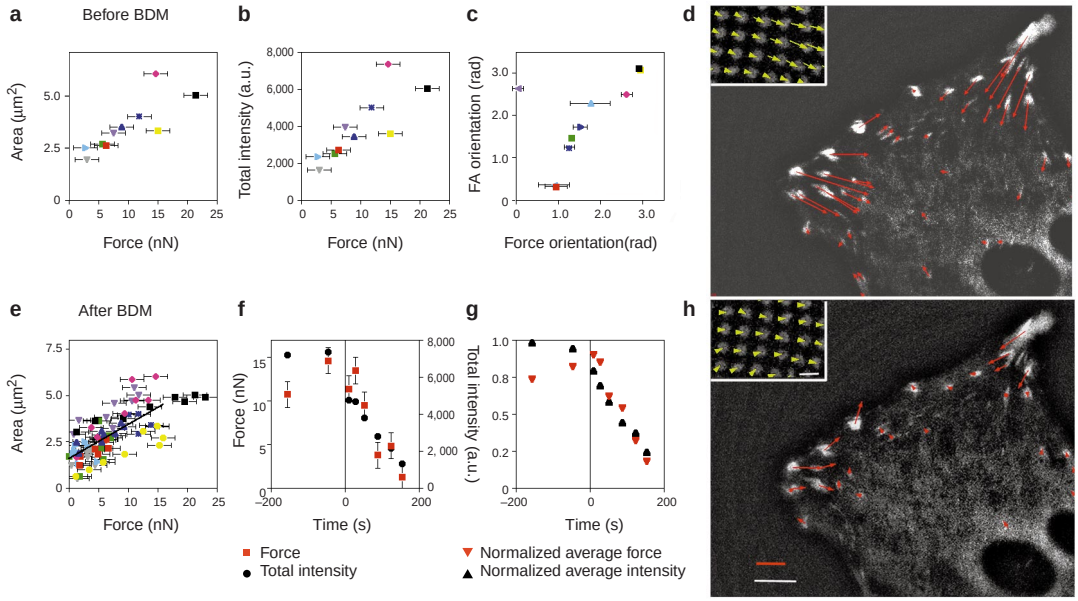

Figure 5 **Correlation between force and focal adhesion structure. a–d**, Before the addition of BDM. **a**, Correlation between force and area of single focal adhesions. **b**, Correlation between force and total fluorescence intensity of single focal adhesions. **c**, Correlation between the direction of the force and the elongation of the focal adhesion. The angles (in radians) were measured relatively to the x axis of the pictures. Each point represents a single focal adhesion from Fig. 5d. Absence of error bars indicates an error below the size of the symbol. **d**, Fluorescence image of a human foreskin fibroblast expressing GFP–vinculin, which localizes to the focal adhesions. The red arrows show the forces transmitted at the focal adhesions. Inset: fluorescence image of the pattern of dots below the left-hand side of the cell; green arrows denote displacements. **e–h**, After the addition of 15 mM 2,3-butanedione monoxime (BDM). **e**, Correlation between the area and force of the focal adhesions of the cell shown in Fig. 5d, at all time points. Each different symbol represents a different focal adhesion. The black line is the correlation line of the linear part of the plot. Its slope defines a stress of 5.5 ± 2 nN μm^{-2} at the focal adhesions. **f**, Time dependence of the relaxation of force (red squares) and total GFP–vinculin intensity (black dots) of a single focal adhesion. **g**, Time dependence of the relaxation of force and total intensity as a normalized average over all focal adhesions. Notice the close correlation between force and total intensity, as both decrease with time. **h**, Same cell as in **d** 2 min after BDM treatment. White bar = 4 μm; red bar = 10 nN; Young's modulus = 12 kPa.

allow the direct visualization and quantification of forces applied to the surface, when combined with elasticity theory. The expression of a GFP fusion protein enables the visualization of individual adhesion sites in live cells and the determination of their dimensions and labelling intensity. The use of an elastomeric substrate was inspired by the elegant studies of Lee *et al.*[14] and Dembo *et al.*[16] We have, however, added features that proved to be essential for assigning specific forces to individual focal adhesions. First, the simultaneous detection of each focal adhesion, and of the associated displacement, allows quantification of the force exerted at distinct focal adhesions. Second, the use of a regular pattern allows direct visualization of distortions, by serving as an internal spatial reference. The pattern is created on the upper layer of the substrate and is firmly anchored to the bulk. This leads to more precise and uniform force quantification, compared to wrinkles or systems in which the markers (e.g. beads) are randomly embedded in the bulk. Last, the calculation of force from the displacements is based on the localization of discrete forces, without assuming the smoothness of the force field (see Methods).

The forces exerted at single focal adhesions in fibroblasts are found to be of the order of 10 nN, with a peak value at 30 nN. The stress measured at the different focal adhesions is constant at 5.5 ± 2 nN μm^{-2}. These results are consistent with previous estimations performed by separately measuring force and focal adhesion density[15,16]. The latter estimations, however, related mainly to forces developed during locomotion, whereas our focus is on the regulation of adhesion by force in stationary cells. The forces during locomotion and their relation to focal adhesion assembly might follow a different regime because adhesion sites have to be disrupted as the cell migrates[18,24].

The quantitative analysis of the dynamic relaxation of force together with the disruption of focal adhesions after the treatment with BDM (Fig. 5e–h) provides new insight into the mechanism relating force and focal adhesion assembly. The striking finding is that the decreases in force and total intensity occur simultaneously. Thus, force and focal adhesion intensity are linked on a time scale that is faster than a few seconds (our experimental resolution). This result puts a clear constraint on the possible mechanisms that have been proposed to account for the relationship between force and focal adhesion assembly. It supports models involving direct conformational changes or molecular rearrangements in focal adhesions upon relaxation or application of force. The mechanism for focal adhesion response to force might be similar to the process that was recently proposed for the assembly of fibronectin under tension, which involves exposing or hiding specific binding sites[25,26]. Recent studies have clearly indicated that integrin signalling depends on cellular contractility[4,5,27,28], but the nature of the 'mechanical switch' or 'sensor' in focal adhesions is still unknown.

In principle, two mechanisms can be considered. The forces applied at focal adhesions might affect the organization and assembly of the multimolecular complexes present in the adhesion sites. Alternatively, the applied force might directly induce unfolding of domains in the integrin itself[29] or in associated molecules[25], thus affecting their binding activity. Can the linear dependence of the assembly on force and the value of the force applied at individual focal adhesions provide information on the nature of this putative mechanosensor? The constant relating force and focal contact area is found to be 5.5 ± 2 nN μm^{-2}. A rough estimate, assuming two-dimensional close packing of integrins, leads to a force per molecule in the adhesion site of the order of 1 pN, similar to the force

exerted by a single myosin molecule[30]. This constitutes a lower limit and is an order of magnitude below the rupture forces that were measured for individual cell–cell adhesion molecules[31] or the force needed reversibly to unfold single domains of proteins like tenascin[32].

However, it has been shown for single proteins that the unfolding rate depends exponentially on the load[33]. Even a force an order of magnitude below rupture can increase the probability of unfolding[34], particularly at a low loading rate[35]. It can therefore be assumed that the force that a cell generates on its adhesion molecules is sufficient to induce a 'feedback response' by locally modulating molecular interactions. The cell could thus use its own contractile apparatus to regulate adhesion in a rapid and local fashion, directing the response exactly to the location at which force must be applied, namely to the binding sites to a rigid surface. Such a mechanism could have developed to, for example, allow the cell to respond differently to ligands that are firmly anchored to a surface than to soluble ligands, or to distinguish between substrates with different rigidities. It would therefore be interesting to unveil the first module affected by force within the focal adhesion complex. □

Methods

Micropatterned elastic surfaces.

The preparation of the micropatterned surfaces was carried out in two steps. First, the negative pattern was prepared using standard optical or electron-beam lithography on solid substrates (Si or GaAs wafers, see below). The solid substrates and their photoresist or polymethylmethacrylate (PMMA) pattern were then used as a mould for patterning the surface of the elastomer[36]. The advantage of the Si–photoresist moulds lies in their ability to be reused many times, avoiding repeated lithography. However, the GaAs–photoresist moulds resulted in a fluorescent pattern embedded in the upper layer of the elastomer, which is easily detected under the cells. This embedding method can thus be used for the patterning of shallow fluorescent markers for focusing marks on the substrate, for example. The different moulds used resulted in substrates of different topography (Fig. 1j). However, the results were similar for the various patterns used. Thus, the pattern was chosen according to the resolution needed.

Si wafers were spin-coated with photoresist (Microposit S1805, Shipley, Marlborough, Massachusetts) for 30 s at 5,000 rpm and cured for 5 min at 80 °C. The thickness of the photoresist coating was 0.3 μm, measured using a stylus surface profiler (Tencor Instruments, Milpitas, California). The photoresist was illuminated with UV light (Mask-aligner, Karl Suss MJB3, Germany); $\lambda = 405$ nm) through a chrome-etched mask with different patterns (Figs 1b, c and 2a) produced by electron-beam lithography. The wafers were washed with developer (Microposit MF-319, Shipley) for 7 s, rinsed with water and dried under a nitrogen stream, followed by an additional curing at 120 °C for 5 min.

GaAs–photoresist moulds were prepared similarly and etched for 2 min, using a 1:1:50 solution of H_3PO_4–H_2O_2–H_20. Si–PMMA moulds were prepared from direct-write electron-beam writing on double-layer PMMA. After development, the wafers were backed at 100 °C for 5 min.

The silicone elastomer was thoroughly mixed with the silicone elastomer curing agent (Sylgard 184, Dow Corning) in a 50:1 ratio in order to obtain a polydimethylsiloxane (PDMS) with a Young's modulus of ~15 kPa, and the mixture was poured on glass coverslips #1. The coated coverslips were then cured at 65 °C for 25 min. The Si–resist moulds were put in contact with the elastomer and cured again at 65 °C overnight. The Si–resist moulds were carefully separated from the coverslips, resulting in a shallow topographic modulation of 0.3 μm at the upper layer of the elastomer (Fig. 1a). The resist thickness determines the depth of the final topographic modulation. In order to avoid known effects of topography on cell spreading and polarization[37], we reduced this depth to the minimum needed for optical detection of the pattern. Fibroblasts plated on parallel lines (pattern of Fig. 1c) with a depth of 0.3 μm did not show any particular orientation, whereas the same pattern with a depth of 1 μm led to a clear polarization of the fibroblasts along the direction of the lines (data not shown).

Alternatively, etched GaAs–photoresist moulds were put in contact with the elastomer. As the adhesion of the photoresist layer to the etched GaAs substrate is weak, the fluorescent photoresist detached during the peeling step (Fig. 1d) and remained embedded in the upper surface of the elastomer, thus creating a fluorescent pattern (Fig. 1f). The yield was lower than for the Si–resist moulds and some of the markers could be missing in the final pattern. This did not have any effect on the final resolution, however, because the coverage of the displacements is dense. The pattern made with Si–resist moulds was observed with standard phase optics (Fig. 1b, c) but it was difficult to resolve the finer patterns under thick parts of the cell. Etched GaAs–photoresist moulds were thus used in experiments with relatively thick cells (e.g. cardiac myocytes) because the photoresist pattern embedded in the elastomer layer can be visualized using either phase-contrast (Fig. 2c, d) or fluorescence (Fig. 1e) (excitation λ = 555 nm; emission λ = 617 nm microscopy.

Characterization of the elastomer.

The bulk elastomer was characterized by suspending known masses on the end of strips, as described by Pelham *et al.*[38]. The elastomer strips return to their original length even after applying a force that induces an elongation of 70% for 24 h. The Poisson ratio was found to be ~0.5 by following changes in volume upon stretching. The Young's modulus varied between 12 kPa and 1000 kPa as the ratio of the silicone elastomer to curing agent varied from 50:1 to 10:1.

Additional calibration of the surface properties was performed *in situ* under the microscope. The patterned elastomer surfaces were immersed in culture medium for several days and a calibrated micropipette was used to deflect the surface. The deflection of the micropipette was measured and translated into a force, together with the deformation of the patterned elastomer (Fig. 1g, h). The distortions of the elastomer with and without embedded markers decay linearly with distance and are proportional to the applied force. Knowing the force applied by the micropipette, the Young's modulus of the elastomer was calculated from the displacements and found to be consistent with the value measured in the bulk. The micropipettes were calibrated by hanging wires of known mass on the tip of the pipettes and measuring the resulting deflection under the microscope[14].

The pipettes were pulled with laser-based programmable micropipette puller (Sutter P-2000; Instruments Company, Novato, CA), and their elastic constant was in the range of 20–50 nN μm^{-1}. The forces applied with the pipettes to the substrates were between 120 nN and 500 nN.

The relaxation time of the patterned elastomer after mechanical perturbation was measured by phase-contrast microscopy using a video system (25 frames per second). The typical time for rapid recoiling to 80% of the distance to the original position was 100 ms, with full relaxation (>95%) occurring within 400 ms.

Calculation of forces at focal adhesions.

The displacement of the elastic substrate under cell traction was reconstructed by processing the phase-contrast images with the 'water' algorithm[20]. N different displacement vectors were obtained by comparing the distorted pattern of dots on a square lattice with its undistorted counterpart recorded after trypsinization (typically, $N = 1000$). We assumed that the cells apply significant cellular forces exclusively at focal adhesion sites, an assumption supported by the fact that displacements were only detected in close proximity to well-developed focal adhesions. Using the 'water' algorithm for the fluorescence images for GFP–vinculin, we find M focal adhesions per cell (typically, $M = 100$).

With a Young's modulus of between 10 kPa and 20 kPa, surface displacements of the order of micrometres resulted from cell traction. As this is considerably smaller than the film thickness (40 μm), the thick polymer film can be assumed to be an elastic halfspace under tangential traction. Video microscopy for monitoring recovery after micropipette traction confirms that the viscoelastic response can be neglected. Detailed considerations of the elasticity of an isotropic halfspace also show that each focal adhesion can be modelled as one point force exerted at the centre of mass, as long as no deformations are picked up within the focal adhesion area itself or its immediate vicinity. The elastic substrate has a Poisson ratio close to 0.5 and so no out-of-plane deformations occur for tangential traction and the entire elastic problem of the substrate surface is two-dimensional. Using the well-known Green function for the upper surface of an elastic halfspace with Poisson ratio of 0.5 under tangential traction[39], one arrives at a set of linear equations of the form $u = G\,F$ that relates the forces F at the site of focal adhesions to the displacements u of the elastic substrate by the action of a matrix G.

We know both u and G and want to find F, and so we have to solve the reverse problem, which is 'ill-posed' owing to the presence of noise. We use zero-order regularization—that is, we minimize $|GF-u|^2 + \lambda^2|F|$ for F using singular value decomposition[40]. The regularization parameter λ is chosen so that the residual norm $|GF - u|^2$ attains the value $2(N–M)\,\sigma^2$, which is its theoretical value if one assumes a Gaussian distribution of the variance σ for the noise in the displacement vector components. Higher order regularization is less appropriate because the force field exerted by focal adhesions cannot be assumed to be smooth in general.

The spatial resolution of measurement of the displacement of the centres of the dots is less than a micrometre. The centre of the dots can be determined with an accuracy below the optical resolution, and we estimate it to be 0.13 μm with a ×100 objective. However, it is not trivial to translate this uncertainty or noise in the displacement measurement to a limit on the force resolution. Our goal was to determine how separate two focal contacts should be in order to measure their respective forces accurately. In order to estimate this, we have added the experimental noise level to a set of known forces (bootstrap)[41] and then retrieved the forces. We found that forces that are 3 μm apart can be reliably retrieved. The error on the force estimate owing to noise is found to be ± 2 nN (U. S. Schwarz *et al.*, unpublished results).

Cells and immunofluorescence staining.

Human foreskin fibroblasts from primary stock (passages 14–28) were grown in Dulbecco's modified eagle's medium (DMEM) supplemented with antibiotics and 10% foetal calf serum. Primary neonatal rat cardiomyocyte and cardiac fibroblasts cell cultures were prepared according to a protocol provided by H. M. Eppenberger (ETH, Zurich, Switzerland)[42]. Fibroblasts were treated on the microscope stage with 15 mM of the inhibitor BDM (Sigma). Immunofluorescence staining was performed as described[20,43].

Digital microscopy of live cells.

The methods for image acquisition were as previously described[19]. For live cell observation, the patterned elastomer substrates, set on coverslips, were mounted into chambers by attaching the coated coverslips to the bottom of 35 mm tissue culture plates with 15 mm diameter holes. The plates were then sterilized by UV for 60 min, washed extensively with PBS and incubated at 4 °C overnight with a 10 μg ml^{-1} solution of fibronectin (Sigma) in PBS. Before plating the cells, the coverslips were washed twice with plating medium and incubated with fresh plating medium for ~1 hour at 37 °C. For microscopic observation, the cells were maintained in DMEM lacking sodium bicarbonate, supplemented with 10% foetal calf serum and buffered with 10 mM HEPES, pH 7.2. Cells were observed with an Axiovert microscope (Zeiss, Oberkochen, Germany) using the DeltaVision acquisition system (Applied Precision, Issaquah, Washington). For live cell experiments, Plan-Apochromat objectives (Zeiss) were used (×100, Ph3/1.3 NA and ×40, Ph3/1.0 NA). The temperature of cells under observation was maintained at 37 °C by temperature control of the oil-immersion objectives, using a heating ring and controller (CT15, Minco, Minneapolis, Minnesota)[12]. Images were processed with Priism software[20].

Expression of GFP–vinculin fusion protein.

Full-length vinculin cDNA was ligated in frame into the GFP expression vector pGZ21 as previously described[20]. Transfection was done by electroporation as previously described[19].

Transmission electron microscopy (TEM)

Cells were cultured for 48 h on the patterned surfaces. The cells were fixed as previously described[44]. After post-fixation, the elastomer was peeled off, while the pattern remained in the embedding material. The samples were than re-embedded and cut, as previously described[44].

RECEIVED 17 AUGUST 2000; REVISED 14 DECEMBER 2000; ACCEPTED 11 JANUARY 2001; PUBLISHED 6 APRIL 2001

1. Yang, J. T., Rayburn, H. & Hynes, R. O. Cell adhesion events mediated by alpha 4 integrins are essential in placental and cardiac development. *Development* **121,** 549–560 (1995).
2. Sheetz, M. P., Felsenfeld, D. P. & Galbraith, C. G. Cell migration: regulation of force on extracellular-matrix–integrin complexes. *Trends Cell Biol.* **8,** 51–54 (1998).
3. Rossiter, H., Alon, R. & Kupper, T. S. Selectins, T-cell rolling and inflammation. *Mol. Med. Today* **3,** 214–222 (1997).
4. Burridge, K. & Chrzanowska-Wodnicka, M. Focal adhesions, contractility, and signaling. *Annu. Rev. Cell. Dev. Biol.* **12,** 463–518 (1996).
5. Bershadsky, A. & Geiger, B. Cytoskeleton-associated anchor and signal transduction proteins. In *Guidebook to the Extracellular Matrix, Anchor, and Adhesion Proteins* (eds Kreis, T. & Vale, R.) 3–11 (Oxford Univ. Press, 1999).
6. Helfman, D. M. *et al.* Caldesmon inhibits nonmuscle cell contractility and interferes with the formation of focal adhesions. *Mol. Biol. Cell* **10,** 3097–3112 (1999).
7. Ingber, D. Integrins as mechanochemical transducers. *Curr. Opin. Cell Biol.* **3,** 841–848 (1991).
8. Yamada, K. M. & Geiger, B. Molecular interactions in cell adhesion complexes. *Curr. Opin. Cell Biol.* **9,** 76–85 (1997).
9. Geiger, B., Yehuda-Levenberg, S. & Bershadsky, A. D. Molecular interactions in the submembrane plaque of cell–cell and cell–matrix adhesions. *Acta Anat. (Basel)* **154,** 46–62 (1995).
10. Abercrombie, M. & Dunn, G. A. Adhesions of fibroblasts to substratum during contact inhibition observed by interference reflection microscopy. *Exp. Cell Res.* **92,** 57–62 (1975).
11. Choquet, D., Felsenfeld, D. P. & Sheetz, M. P. Extracellular matrix rigidity causes strengthening of integrin–cytoskeleton linkages. *Cell* **88,** 39–48 (1997).
12. Riveline, D. *et al.* Externally applied local mechanical force induces growth of focal contacts by a mDia1-dependent and ROCK-independent mechanism. *J. Cell Biol.* (in the press).
13. Harris, A. K., Wild, P. & Stopak, D. Silicone rubber substrata: a new wrinkle in the study of cell locomotion. *Science* **208,** 177–179 (1980).
14. Lee, J., Leonard, M., Oliver, T., Ishihara, A. & Jacobson, K. Traction forces generated by locomoting keratocytes. *J. Cell Biol.* **127,** 1957–1964 (1994).
15. Galbraith, C. G. & Sheetz, M. P. A micromachined device provides a new bend on fibroblast traction forces. *Proc. Natl Acad. Sci. USA* **94,** 9114–9118 (1997).
16. Dembo, M. & Wang, Y. L. Stresses at the cell-to-substrate interface during locomotion of fibroblasts. *Biophys. J.* **76,** 2307–2316 (1999).
17. Burton, K. & Taylor, D. L. Traction forces of cytokinesis measured with optically modified elastic substrata. *Nature* **385,** 450–454 (1997).
18. Burton, K., Park, J. H. & Taylor, D. L. Keratocytes generate traction forces in two phases. *Mol. Biol. Cell* **10,** 3745–3769 (1999).
19. Zamir, E. *et al.* Dynamics and segregation of cell-matrix adhesions in cultured fibroblasts. *Nature Cell Biol.* **2,** 191–196 (2000).
20. Zamir, E. *et al.* Molecular diversity of cell–matrix adhesions. *J. Cell Sci.* **112,** 1655–1669 (1999).
21. Dembo, M., Oliver, T., Ishihara, A. & Jacobson, K. Imaging the traction stresses exerted by locomoting cells with the elastic substratum method. *Biophys. J.* **70,** 2008–2022 (1996).
22. Nobes, C. D. & Hall, A. Rho, rac, and cdc42 GTPases regulate the assembly of multimolecular focal complexes associated with actin stress fibers, lamellipodia, and filopodia. *Cell* **81,** 53–62 (1995).
23. Cramer, L. P. & Mitchison, T. J. Myosin is involved in postmitotic cell spreading. *J. Cell Biol.* **131,** 179–189 (1995).
24. Beningo, K. A., Dembo, M., Kaverina, I. N., Small, J. V. & Wang, Y.-L. Nascent focal adhesions are responsible for the generation of strong traction forces in migrating cells. *Mol. Biol. Cell* **11,** 4 (2000).
25. Zhong, C. *et al.* Rho-mediated contractility exposes a cryptic site in fibronectin and induces fibronectin matrix assembly. *J. Cell Biol.* **141,** 539–551 (1998).
26. Shaub, A. Unravelling the extracellular matrix. *Nature Cell Biol.* **1,** E173–E175 (2000).
27. Howe, A., Aplin, A. E., Alahari, S. K. & Juliano, R. L. Integrin signaling and cell growth control. *Curr. Opin. Cell Biol.* **10,** 220–231 (1998).
28. Felsenfeld, D. P., Schwartzberg, P. L., Venegas, A., Tse, R. & Sheetz, M. P. Selective regulation of integrin–cytoskeleton interactions by the tyrosine kinase Src. *Nature Cell Biol.* **1,** 200–206 (1999).
29. Chicurel, M. E., Chen, C. S. & Ingber, D. E. Cellular control lies in the balance of forces. *Curr. Opin. Cell Biol.* **10,** 232–239 (1998).
30. Finer, J. T., Mehta, A. D. & Spudich, J. A. Characterization of single actin–myosin interactions. *Biophys. J.* **68,** 291S–296S (1995).
31. Benoit, M., Gabriel, D., Gerish, G. & Gaub, H. E. Discrete interactions in cell adhesion measured by single-molecule force spectroscopy. *Nature Cell Biol.* **2,** 313–317 (2000).
32. Oberhauser, A. F., Marszalek, P. E., Erickson, H. P. & Fernandez, J. M. The molecular elasticity of the ECM protein tenascin. *Nature* **393,** 181–185 (1998).
33. Carrion-Vazquez, M. *et al.* Mechanical and chemical unfolding of a single protein: a comparison. *Proc. Natl Acad. Sci. USA* **96,** 3694–3699 (1999).
34. Bell, G. I. Models for the specific adhesion of cells to cells. *Science* **200,** 618–627 (1978).
35. Merkel, R., Nassoy, P., Leung, A., Ritchie, K. & Evans, E. Energy landscapes of receptor–ligand bonds explored with dynamic force spectroscopy. *Nature* **397,** 50–53 (1999).
36. Chen, C. S., Mrksich, M., Huang, S., Whitesides, G. M. & Ingber, D. E. Geometric control of cell life and death. *Science* **276,** 1425–1428 (1997).
37. Dow, J. A., Clark, P., Connolly, P., Curtis, A. S. & Wilkinson, C. D. Novel methods for the guidance and monitoring of single cells and simple networks in culture. *J. Cell Sci.* (Suppl.) **8,** 55–79 (1987).
38. Pelham, R. J. Jr & Wang, Y. Cell locomotion and focal adhesions are regulated by substrate flexibility. *Proc. Natl Acad. Sci. USA* **94,** 13661–13665 (1997).
39. Landau, L. D. & Lifshitz, E. M. *Course of Theoretical Physics: Theory of Elasticity.* Vol. 7, 2nd edn (Pergamon Press, Oxford, 1970).
40. Press, W. H., Teukolsky, S. A., Vetterling, W. T. & Flannery, B. P. *Numerical recipes in FORTRAN. The art of scientific computing.* 2nd edn (Cambridge Univ. Press, 1992).
41. Efron, B. & Tibshirani, R. J. *Monographs on Statistics and Applied Probability: An Introduction to the Bootstrap.* Vol. 57 (Chapman and Hall, 1993).
42. Harder, B. A., Hefti, M. A., Eppenberger, H. M. & Schaub, M. C. Differential protein localization in sarcomeric and nonsarcomeric contractile structures of cultured cardiomyocytes. *J. Struct. Biol.* **122,** 162–175 (1998).
43. Katz, B. Z. *et al.* Physical state of the extracellular matrix regulates the structure and molecular composition of cell–matrix adhesions. *Mol. Biol. Cell* **11,** 1047–1060 (2000).
44. Levenberg, S., Katz, B. Z., Yamada, K. M. & Geiger, B. Long-range and selective autoregulation of cell–cell or cell–matrix adhesions by cadherin or integrin ligands. *J. Cell Sci.* **111,** 347–357 (1998).

ACKNOWLEDGEMENTS

We wish to thank E. Zamir and E. Moses for illuminating discussions and technical assistance. This study was supported by the Israel Science Foundation, administrated by the Israel Academy of Science and the Minerva Foundation. B.G. holds the E. Neter chair for Cell and Tumor Biology. L.A. is incumbent of the Dorothy and Patrick Gorman Professorial chair of Biological Ultrastructure. U.S.S. was supported by the Minerva Foundation. A. B. holds the J. Moss chair of Biomedical Research.

Correspondence and requests for materials should be addressed to B.G. Supplementary Information is available on *Nature Cell Biology*'s website (http://cellbio.nature.com).

Movie 1 **Two beating cardiac myocytes on the micropatterned elastomer.** Beating is reconstructed from pictures acquired either in the contracted or the relaxed phase. The border between patterned and non-patterned elastomer can be seen in the lower part of the picture.

Movie 2 **A cardiac myocyte plated on the micropatterned elastic substrate.** Reconstruction from pictures acquired sequentially either in the relaxed or the contracted phase. White crosses indicate regions of contraction; black cross in the upper left shows a non-disturbed location.